EPJ Web of Conferences **3**, 03004 (2010)
DOI:10.1051/epjconf/20100303004

Recent results from the G^0 experiment

J.S. Real[11,a], D. Androić[1], D. S. Armstrong[2], J. Arvieux[3,b], S. L. Bailey[2], D. H. Beck[4], E. J. Beise[5], J. Benesch[6], F. Benmokhtar[57], L. Bimbot[3], J. Birchall[8], P. Bosted[6], H. Breuer[5], C. L. Capuano[2], Y.-C. Chao[6], A. Coppens[8], C. A. Davis[9], C. Ellis[5], G. Flores[10], G. Franklin[7], C. Furget[11], D. Gaskell[6], M. T. W. Gericke[8], J. Grames[6], G. Guillard[11], J. Hansknecht[6], T. Horn[6], M. Jones[6], P. M. King[12], W. Korsch[13], S. Kox[11], L. Lee[8], J. Liu[14], A. Lung[6], J. Mammei[15], J. W. Martin[16], R. D. McKeown[14], A. Micherdzinska[16], M. Mihovilovic[17], H. Mkrtchyan[18], M. Muether[4], W. T. H. van Oers[8], S. A. Page[8], V. Papavassiliou[10], S. F. Pate[10], S. K. Phillips[2], P. Pillot[11], M. L. Pitt[15], M. Poelker[6], B. Quinn[7], W. D. Ramsay[8], J. Roche[12], P. Roos[5], J. Schaub[10], T. Seva[1], N. Simicevic[19], G. R. Smith[6], D. T. Spayde[20], M. Stutzman[6], R. Suleiman[156], V. Tadevosyan[18], M. Versteegen[11], E. Voutier[11], W. Vulcan[6], S. P. Wells[19], S. E. Williamson[4], and S. A. Wood[6]

[1] Department of Physics, University of Zagreb, Zagreb HR-41001 Croatia
[2] Department of Physics, College of William and Mary, Williamsburg, VA 23187 USA
[3] Institut de Physique Nucléaire d'Orsay, Université Paris-Sud, F-91406 Orsay Cedex FRANCE
[4] Loomis Laboratory of Physics, University of Illinois, Urbana, IL 61801 USA
[5] Physics Department, University of Maryland, College Park, MD 20742 USA
[6] Thomas Jefferson National Accelerator Facility, Newport News, VA 23606 USA
[7] Department of Physics, Carnegie Mellon University, Pittsburgh, PA 15213 USA
[8] Department of Physics, University of Manitoba, Winnipeg, MB R3T 2N2 CANADA
[9] TRIUMF, Vancouver, BC V6T 2A3 CANADA
[10] Physics Department, New Mexico State University, Las Cruces, NM 88003 USA
[11] LPSC, Université Joseph Fourier Grenoble 1, CNRS/IN2P3, Institut Polytechnique de Grenoble, Grenoble, FRANCE
[12] Department of Physics and Astronomy, Ohio University, Athens, OH 45701 USA
[13] Department of Physics and Astronomy, University of Kentucky, Lexington, KY 40506 USA
[14] Kellogg Radiation Laboratory, California Institute of Technology, Pasadena, CA 91125 USA
[15] Department of Physics, Virginia Tech, Blacksburg, VA 24061 USA
[16] Department of Physics, University of Winnipeg, Winnipeg, MB R3B 2E9 CANADA
[17] Jožef Stefan Institute, 1000 Ljubljana, SLOVENIA
[18] Yerevan Physics Institute, Yerevan 375036 ARMENIA
[19] Department of Physics, Louisiana Tech University, Ruston, LA 71272 USA
[20] Department of Physics, Hendrix College, Conway, AR 72032 USA

Abstract. We have measured parity violating asymmetries in elastic electron-proton and quasi-elastic electron-deuteron scattering at backward electron angle. These measurements have been done at two momentum transfers : $Q^2 = 0.22$ and 0.63 $(GeV/c)^2$. Together with our previous forward angle measurement [1], we can extract strange quark contributions to the electromagnetic form factors of the nucleon, as well as nucleon axial form factor coming from the neutral weak interaction. The results indicate a strange quark magnetic contribution close to zero at these Q^2, and a possible non zero strange quark electric contribution for the high Q^2. The first Q^2 behavior measurement of the nucleon axial form factor in elastic electron scattering shows a good agreement with radiative corrections calculated at $Q^2 = 0$ and with a dipole form using the axial mass determined in neutrino scattering.

1 Introduction

At intermediate energy, the nucleon is described by three valence quarks plus a sea of quark-antiquark pairs and gluons. One of the main questions, since the last 20 years, is how the nucleon properties, like the mass, the spin or the magnetic moment, are built up from its quark and gluon constituents. QCD can not described such a bound system using perturbation theory at this scale, and treatment of non valence quark with the correct mass is a challenge to lattice QCD. The picture where valence QCD quarks contribute exclusively is not reliable. It is obvious for the mass, since the three valence quarks represent only at most 1.5% of the nucleon mass. But it is also visible for the spin where only about 30% of the proton spin is carried by the spin of its quarks while relativistic constituent quark model predict 60%, with the rest carried by orbital angular momentum. Something beyond the valence quark should play an important role. A large number of experiments focused on the study of the sea quark-antiquark pairs contribution

[a] e-mail: real@in2p3.fr
[b] Deceased

to the nucleon properties. We will describe here measurements of the strange quark contributions to the charge and magnetization distributions of the nucleon. Since nucleon does not have valence strange quark, this electromagnetic contribution is exclusively part of the sea.

2 Electromagnetic structure of the nucleon

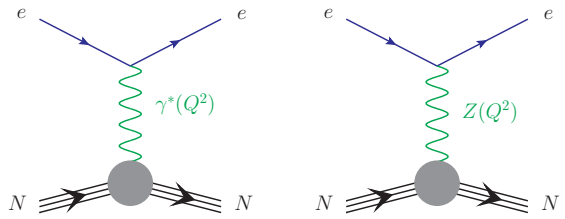

Fig. 1. Diagrams contributing to the elastic electron-nucleon scattering.

Electromagnetic structure of the nucleon is best probed using lepton scattering. We focus here in the elastic and quasi-elastic electron scattering on the nucleon. In the Born approximation, this scattering is described by virtual photon (γ^*) exchange for the electromagnetic part, and neutral boson Z^0 exchange for the weak part (since we are focusing on elastic scattering, only neutral currents contribute). The leptonic current is well described by the quantum electrodynamics (QED), but for the hadronic current, one has to take into account the internal nucleon's structure by using two structure functions (form factors in the case of elastic scattering). The scattering amplitudes $\mathcal{M}_\gamma$ and $\mathcal{M}_Z$ can be written :

$$\mathcal{J}_\mu^{(\gamma,e)} = -e\bar{u}\gamma^\mu u \tag{1a}$$

$$\mathcal{J}_\nu^{(\gamma,N)} = e\bar{v}\left[F_1^{\gamma,N}\gamma_\nu + i\frac{F_2^{\gamma,N}}{2m}\sigma_{\nu\delta}q^\delta\right]v \tag{1b}$$

$$\mathcal{M}_\gamma = \mathcal{J}_\mu^{(\gamma,e)}\frac{g^{\mu\nu}}{q^2}\mathcal{J}_\nu^{(\gamma,N)} \tag{1c}$$

$$\mathcal{J}_\mu^{(Z,e)} = \frac{-g}{4\cos\theta_W}\bar{u}\gamma_\mu\left(c_V^e + c_A^e\gamma^5\right)u \tag{2a}$$

$$\mathcal{J}_\nu^{(Z,N)} = \frac{g}{4cos\theta_W}\bar{v}\left(F_1^{(Z,N)}\gamma_\nu + \frac{iF_2^{(Z,N)}}{2m}\sigma_{\nu\delta}q^\delta + G_A^{(Z,N)}\gamma_\nu\gamma^5 + \frac{G_P^{(Z,N)}}{m}\gamma^5 q_\nu\right)v \tag{2b}$$

$$\mathcal{M}_Z = \mathcal{J}_\mu^{(Z,e)}\frac{g^{\mu\nu} - q^\mu q^\nu/m_Z^2}{q^2 - m_Z^2}\mathcal{J}_\nu^{(Z,N)} \tag{2c}$$

where m is the nucleon mass, θ_W is the weak mixing angle. The γ^* is associated to a vector coupling at both leptonic and hadronic vertex and we define the Dirac (F_1^γ) and the Pauli (F_2^γ) form factors for the hadronic vertex (eq. 1b). On the other hand, Z^0 coupling involves a superposition of vector and axial currents. It implies axial couplings, c_A^e in the leptonic vertex (eq. 2a) and axial $G_A^{(Z,N)}$ and pseudoscalar $G_P^{(Z,N)}$ form factors in the hadronic one (2b) in addition to the Dirac (F_1^Z) and the Pauli (F_2^Z) weak vector form factors. F_1 and F_2 only depend on Q^2 which is the momentum transfer between the electron and the nucleon. It is useful to define the electric (E) and magnetic (M) Sachs form factors [2] which are a linear combination of the Pauli and Dirac ones :

$$G_E^{\gamma,N} = F_1^{\gamma,N} - \tau F_2^{\gamma,N} \qquad G_M^{\gamma,N} = F_1^{\gamma,N} + F_2^{\gamma,N}$$
$$G_E^{Z,N} = F_1^{Z,N} - \tau F_2^{Z,N} \qquad G_M^{Z,N} = F_1^{Z,N} + F_2^{Z,N}$$

where $\tau = Q^2/4m^2$. In the Breit frame and in a non relativistic case, these form factors can be linked to the Fourier transform, respectively, of the charge and magnetization spatial distributions. At $Q^2 = 0$, these form factors are normalized to the electric charge and magnetic moment of the nucleon.

$$G_E^p \to 1 \qquad G_E^n \to 0$$
$$G_M^p \to \mu_p = 2.79 \qquad G_M^n \to \mu_n = -1.91$$

The elastic electron nucleon scattering is the coherent sum of the electromagnetic $\mathcal{M}_\gamma$ and neutral weak $\mathcal{M}_Z$ scattering amplitudes :

$$\begin{aligned}\sigma_{ep} &= \left|\mathcal{M}_\gamma + \mathcal{M}_Z\right|^2 \\ &= \left|\mathcal{M}_\gamma\right|^2 + 2\Re e\left(\mathcal{M}_\gamma\mathcal{M}_Z^*\right) + |\mathcal{M}_Z|^2 \\ &= (\cdots)\frac{\alpha^2}{Q^4} + (\cdots)G_f\frac{\alpha}{Q^2} + (\cdots)G_f^2\end{aligned} \tag{3}$$

For small momentum transfer $Q^2 < 1(GeV/c)^2$, Q^2 is negligible compare to the Z^0's mass, then the Z^0 boson's propagator (2c) is proportional to $1/M_Z^2$. The scattering amplitude $\mathcal{M}_Z$ is then proportional to $G_F/2 \simeq 0.5.10^{-6}$ (with Fermi constant $G_F = \frac{g^2}{8M_Z^2\cos^2\theta_W}$), whereas $\mathcal{M}_\gamma$ is $4\pi\alpha/Q^2 \simeq 0.1$. This means that the third term of eq. 3 is completely negligible and that the Z^0 effect only contributes in the interference term $\Re e\left(\mathcal{M}_\gamma\mathcal{M}_Z^*\right)$ for about :

$$\frac{\Re e\left(\mathcal{M}_\gamma\mathcal{M}_Z^*\right)}{\left|\mathcal{M}_\gamma\right|^2} \propto \frac{G_f}{\sqrt{2}\pi\alpha} \simeq 0.03\% \tag{4}$$

3 Quark flavors decomposition

Since gluons do not have electric charge and can not interact by weak interaction, the γ^* and the Z^0 in the elastic eN scattering can only interact with the quarks. We can then decompose the electromagnetic and weak currents upon the quark flavors, and so the electromagnetic and axial form factors. If we assume that only the three lightest flavors contribute and under the charge symmetry

assumption, u quark contribution in the proton is the same as the d quark contribution in the neutron and vice versa ($G_{E,M}^{u,p} = G_{E,M}^{d,n}$, $G_{E,M}^{d,p} = G_{E,M}^{u,n}$, and $G_{E,M}^{s,p} = G_{E,M}^{s,n}$ [3]), we can write :

$$\begin{aligned} G_{E,M}^{\gamma,p} &= \frac{2}{3}G_{E,M}^{u} - \frac{1}{3}G_{E,M}^{d} - \frac{1}{3}G_{E,M}^{s} \\ G_{E,M}^{\gamma,n} &= \frac{2}{3}G_{E,M}^{d} - \frac{1}{3}G_{E,M}^{u} - \frac{1}{3}G_{E,M}^{s} \end{aligned} \tag{5}$$

$$\begin{aligned} G_{E,M}^{Z,p} &= g_V^u G_{E,M}^{u} + g_V^d G_{E,M}^{d} + g_V^s G_{E,M}^{s} \\ G_{E,M}^{Z,n} &= g_V^u G_{E,M}^{d} + g_V^d G_{E,M}^{u} + g_V^s G_{E,M}^{s} \end{aligned} \tag{6}$$

where $g_V^f = 2T_3^f - 4Q_f \sin^2\theta_W$ and $g_A^f = -2T_3^f$ are the weak vector and weak axial charges for quark $f = u, d, s$ (see table 1). By combining equations (5) and (6), strange quark contributions appear explicitly with only electroweak nucleon form factors :

$$\begin{aligned} G_{E,M}^{Z,p} &= \xi_V^p G_{E,M}^{\gamma,p} + \xi_V^n G_{E,M}^{\gamma,n} + \xi_V^{(0)} G_{E,M}^{s} \\ G_{E,M}^{Z,n} &= \xi_V^n G_{E,M}^{\gamma,p} + \xi_V^p G_{E,M}^{\gamma,n} + \xi_V^{(0)} G_{E,M}^{s} \end{aligned} \tag{7}$$

with at tree level :

$$\begin{aligned} \xi_V^p &= 2g_V^u + g_V^d \\ \xi_V^n &= g_V^u + 2g_V^d \\ \xi_V^{(0)} &= g_V^u + g_V^d + g_V^s \end{aligned} \tag{8}$$

Knowing the electromagnetic form factors on proton $G_{E,M}^{\gamma,p}$ and neutron $G_{E,M}^{\gamma,n}$ one has only to measure the weak form factors on the proton $G_{E,M}^{Z,p}$ to accessed the strange quark electric and magnetic contributions.

Fermions (f)	g_V^f	g_A^f	Q_f	T_3^f
u	$1 - \frac{8}{3}\sin^2\theta_W$	-1	$\frac{2}{3}$	1/2
d, s	$-1 - \frac{4}{3}\sin^2\theta_W$	1	$-\frac{1}{3}$	-1/2

Table 1. Vector and axial weak charges for fermions in the S.M. at tree level

4 Electromagnetic form factors

Electromagnetic form factors of the proton and the neutron have been extensively studied these last forty years. This results in a large amount of experimental measurements which have been performed using two different techniques. The first one is the Rosenbluth separation. Since the form factors depend only of the momentum transfers, the elastic cross section is measured twice, at the same Q^2 but at different electron incident energy and scattered angle, given different linear combination of G_E and G_M :

$$\frac{d\sigma}{d\Omega} = \left(\frac{d\sigma}{d\Omega}\right)_{Mott} \frac{\epsilon G_E^2 + \tau G_M^2}{\epsilon(1+\tau)} \tag{9}$$

with $\tau = \frac{Q^2}{4m^2}$ and $\epsilon = \frac{1}{1+2(1+\tau)\tan^2(\theta_e/2)}$. The second technique is to measure the ratio G_E/G_M in single or double polarization experiments. Both techniques give different results. The actual explanation for this disagreement is the effect of the two photon exchange amplitude which may be not negligible for $Q^2 \simeq 1\,(GeV/c)^2$. The two photon exchange would affect more the Rosenbluth data than the polarization one (see ref. [4] and references therein).

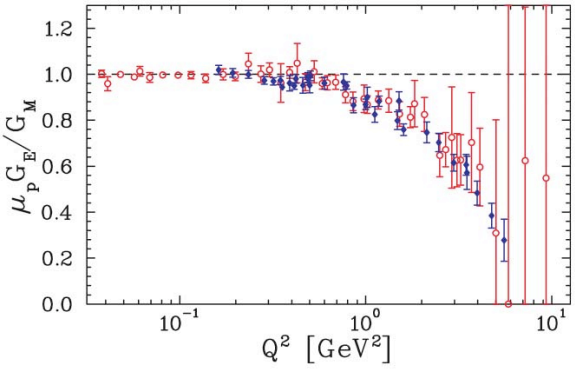

Fig. 2. Electric and magnetic proton form factor ratio corrected for the two photons exchange. Figure is taken from reference [4].

The neutron electric form factor is less constraint for two reasons. Firstly there is no neutron target, secondly electric charge is zero and then measurements are mainly dominated by magnetic moment which prevent to measure the electric form factor accurately. Most precise measurements of the neutron's electric form factor come from the polarization experiments which provide the electric to magnetic ratio.

All these measurements, once corrected for two photons exchange, allow a good determination of electric and magnetic form factor for proton and neutron. To predict them at all Q^2, we use a Q^2 parameterization of the data. The most common one is the dipole form, defined by :

$$G_M^N/\mu_N = G_E^p = G_D = \frac{1}{\left(1 + \frac{Q^2}{\Lambda^2}\right)^2} \quad \text{with } \Lambda = 0.71(GeV/c)^2 \tag{10}$$

This form is not suitable for electric neutron form factor for which the Galster form [5] is used :

$$G_E^n = -\frac{\mu_n \tau}{1 + B\tau} G_D \quad \text{with B=5.6.} \tag{11}$$

The dipole and Galster's parameterization reproduces correctly the data at low Q^2, but not the ratio $\mu G_E/G_M$ above 0.5 $(GeV/c)^2$. For the G^0 we use the Kelly's parameterization [6] which described correctly the form factors with the minimal set of parameters :

$$G(Q^2) = \frac{\sum_{i=0}^{n} a_i \tau^i}{1 + \sum_{i=1}^{n+2} b_i \tau^i} = \frac{1 + a_1\tau}{1 + b_1\tau + b_2\tau^2 + b_3\tau^3} \tag{12}$$

With n=1 and $a_0 = 1$, four parameters only (a_1, b_1, b_2, b_3) are necessary. For G_{En}, we have to use the same expression as the one of Galster [5], taken also μ_n and B as parameters.

5 Axial form factor

Axial form factor can be decompose the same way on the quarks flavors, for both proton and neutron :

$$\begin{aligned} G_A^{Z,p} &= g_A^u G_A^u + g_A^d G_A^d + g_A^s G_A^s \quad = -G_A^u + G_A^d + G_A^s \\ G_A^{Z,n} &= g_A^u G_A^d + g_A^d G_A^u + g_A^s G_A^s \quad = -G_A^d + G_A^u + G_A^s \end{aligned}$$

One can then write for the nucleon :

$$G_A^{Z,N} = -\tau_z G_A^{T=1} + g_A^s G_A^s \tag{13}$$

where $\tau_z = 1$ for proton and -1 for neutron and $G_A^{T=1} = G_A^u - G_A^d$ is the axial isovector form factor. $G_A^{Z,N}$ is the axial form factor measured in (anti-)neutrino scattering for which only the weak interaction contributes (no virtual photon exchange). When going to electron scattering, electroweak radiative corrections need to be included due to the electron charge. Axial form factor for electron scattering can be rewrite in a more general way :

$$G_A^{e,N} = \tau_3 \xi_A^{T=1} G_A^{T=1} + \sqrt{3}\xi_A^{T=0} G_A^{T=0} + \xi_A^{(0)} G_A^s \tag{14}$$

with :

$$\begin{aligned} \xi_A^{T=1} &= g_A^u - g_A^d \\ \xi_A^{T=0} &= g_A^u + g_A^d \\ \xi_A^{(0)} &= g_A^u + g_A^d + g_A^s \end{aligned} \tag{15}$$

At tree level $g_A^u = -1$ and $g_A^d = g_A^s = 1$, leading to $\xi_A^{T=1} = -2$, $\xi_A^{T=0} = 0$ and $\xi_A^{(0)} = 1$, and then $G_A^{e,N} = G_A^{Z,N}$.

At $Q^2 = 0$, the isovector form factor $G_A^{T=1}$ is linked to the β decay of the neutron, the isoscalar term $G_A^{T=0}$ to the β decay of the hyperon [7] and the isoscalar strange term G_A^s reduces to Δs, which is the fraction of the nucleon spin carried by the strange quark s and $\bar{s}$:

$$\begin{aligned} G_A^{T=1}(Q^2 = 0) &= \frac{g_A}{g_V} = -1.2695 \\ G_A^{T=0}(Q^2 = 0) &= (0.585 \pm 0.025)/6 \\ G_A^s(Q^2 = 0) &= \Delta s = -0.8 \pm 0.4 \end{aligned} \tag{16}$$

Δs is not well known, it ranges from 0.0 to -0.14, and we use the value of reference [8]. The axial form factor Q^2 dependance has been determined, using a dipole form, from νN and νD scattering [9] :

$$G_A^{Z,N}(Q^2) = G_A^{Z,N}(0) \frac{1}{\left(1 + \frac{Q^2}{M_A^2}\right)^2} \quad \text{with} \quad M_A = 1.014 \pm 0.014 \tag{17}$$

6 Parity violation asymmetry

To get the strange quark contribution to the electromagnetic properties of the nucleon, one has to measure the weak electric and magnetic form factors of the proton (see section 3). In elastic electron scattering cross section, this measurement is not possible for small momentum transfers due to the weakness of the weak interaction (see section 2). To access the Z_0 interaction, we use the fact that weak interaction violate the parity. In that case the polarized cross section is different wherever the initial electrons are in (+) or (-) helicity state. Measuring the difference of these cross sections leads to the parity violating asymmetry which is given using equation 3. Neglecting $|\mathcal{M}_Z|^2$ compared to $\Re e^{+-}\left(\mathcal{M}_\gamma \mathcal{M}_Z^*\right)$ and $\Re e^{+-}\left(\mathcal{M}_\gamma \mathcal{M}_Z^*\right)$ compared to $|\mathcal{M}^\gamma|^2$, and due to the fact that the electromagnetic interaction does not violate the parity ($\left|\mathcal{M}_\gamma^+\right|^2 = \left|\mathcal{M}_\gamma^-\right|^2$), the asymmetry can be written :

$$A_{PV} = \frac{\sigma_{ep}^+ - \sigma_{ep}^-}{\sigma_{ep}^+ + \sigma_{ep}^-} = \frac{\Re e^-\left(\mathcal{M}_\gamma \mathcal{M}_Z^*\right) - \Re e^+\left(\mathcal{M}_\gamma \mathcal{M}_Z^*\right)}{\left|\mathcal{M}_\gamma\right|^2} \tag{18}$$

and using the expression of scattering amplitude in terms of form factors, the asymmetry becomes :

$$A_{PV}^N = -f \frac{\epsilon G_E^{\gamma,N} G_E^{Z,N} + \tau G_M^{\gamma,N} G_M^{Z,N} - f_W \epsilon' G_M^{\gamma,N} G_A^{e,N}}{\epsilon G_E^{\gamma,N\,2} + \tau G_M^{\gamma,N\,2}} \tag{19}$$

with kinematical factors :

$$\begin{aligned} f &= \frac{G_F Q^2}{4\sqrt{2}\pi\alpha} \\ f_W &= \left(1 - 4sin^2\theta_W\right) \\ \tau &= Q^2/(4M_N^2) \\ \epsilon &= (1 + 2(1+\tau)\tan^2(\theta_e/2))^{-1} \\ \epsilon' &= \sqrt{\tau(1+\tau)(1-\epsilon^2)} \end{aligned} \tag{20}$$

Then replacing weak form factors by their expression from equation 7, parity violating asymmetry can be expressed in terms of strange quark contributions :

$$A_{PV}^p = A_0^p + A_E^p G_E^s + A_M^p G_M^s + A_A^p G_A^{e,p} \tag{21}$$

with :

$$\begin{aligned} A_0^p &= -f_A \left[\epsilon G_E^{\gamma,p}\left(\xi_V^p G_E^{\gamma,p} + \xi_V^n G_E^{\gamma,n}\right) \right. \\ &\qquad \left. + \tau G_M^{\gamma,p}\left(\xi_V^p G_M^{\gamma,p} + \xi_V^n G_M^{\gamma,n}\right)\right] \\ A_E^p &= -f_A \left[\epsilon G_E^{\gamma,p} \xi_V^{(0)}\right] \\ A_M^p &= -f_A \left[\tau G_M^{\gamma,p} \xi_V^{(0)}\right] \\ A_A^p &= +f_A \left[(1 - 4\sin^2\theta_W)\epsilon' G_M^{\gamma,p}\right] \end{aligned} \tag{22}$$

and :

$$f_A = \frac{G_F Q^2}{4\pi\sqrt{2}\alpha(\epsilon(G_E^{\gamma,p})^2 + \tau(G_M^{\gamma,p})^2)}$$

The coefficients A_0^p, A_E^p, A_M^p and A_A^p can be calculated with relatively small errors by using a parameterization for electromagnetic form factors. The axial part can be broken down in two terms, one isovector and one including isoscalar and axial strange parts (see eq. 14). The non isovector part

is small and it is convenient to include it in the A_0 coefficient allowing to keep only the isovector part $G_A^{T=1}$ in the axial term. Doing three measurements in different kinematical conditions will allow to extract the strange quark contributions and the isovector axial term which include specific radiative corrections in electron scattering. These measurements should be done at the same Q^2 and different kinematics providing sizeable differences in the coefficients. The two common settings are the measurement of parity violating asymmetry on hydrogen at small scattered electron angle (the forward angle, $\theta_e < 15^\circ$) and at large scattered angle (the backward angle, $\theta_e > 90^\circ$). These measurements allow to separate the electric and magnetic term if one use a theoretical prediction for G_A^e.

A third measurement with enough sensitivity to G_A^e has to be done on deuterium target measuring the quasi-elastic scattering on proton and neutron. In the static approximation (neglecting nuclear force between nucleons), the parity violating asymmetry on deuteron can be written :

$$A_{PV}^{QE} = \frac{\sigma_p A_{PV}^p + \sigma_n A_{PV}^n}{\sigma_p + \sigma_n}$$

We can go one step further, including a momentum distribution for the nucleons and use a y-scaling model [10,11,12] for the cross section. A preferred way, used here, is to use a model calculation of the nucleon-nucleon interaction [13,14,15]. In this model the one-body electromagnetic and weak currents include lowest order relativistic corrections, and two-body contributions are included in the electromagnetic current using π exchange (which is dominant) and other shorter range currents. Intermediate state Δ excitation is also taken into account. The calculation is based on the Argonne V18 potential [16] for the parity conservating interaction, and the "DDH" parameterization [17] of the parity violating potential. The Kelly's parameterization [6] is used for the electromagnetic form factors. The deuteron quasi-elastic parity violating asymmetry is written [18,19,20] :

$$A_{PV}^{QE} = f\frac{v_L R_L^Z(\mathbf{q},\omega) + v_T R_T^Z(\mathbf{q},\omega) + v_{T'} R_{T'}^A(\mathbf{q},\omega)}{v_L R_L^\gamma(\mathbf{q},\omega) + v_T R_T^\gamma(\mathbf{q},\omega)} \quad (23)$$

where f is defined in equation 20, $(\mathbf{q},\omega)$ is the momentum four-vector of the virtual photon and :

$$v_L = \left(\frac{Q^2}{q^2}\right)^2 \qquad v_T = \frac{1}{2}\left|\frac{Q^2}{q^2}\right| + \tan^2\frac{\theta_e}{2}$$
$$v_{T'} = \left[\left|\frac{Q^2}{q^2}\right| + \tan^2\frac{\theta_e}{2}\right]^{1/2}\tan\frac{\theta_e}{2} \quad (24)$$

The parity violating response functions can be split up with explicit strange quark pieces :

$$\begin{aligned} R_L^Z &= R_L^V + R_L^s \\ R_T^Z &= R_T^V + R_T^{cs} + R_T^s \\ R_{T'}^A &= \left(R_{LT}^A\right)^{00} + \left(R_{LT}^A\right)^{01} + \left(R_{LT}^A\right)^{10} + \left(R_{LT}^A\right)^{11} \end{aligned} \quad (25)$$

The indices in the axial response function are the isospin of the axial and electromagnetic currents respectively. R_T^{cs} result from a convection current that contribute to the charge and thus contribute to G_E^s. The asymmetry can then be written as equation 21 with :

$$\begin{aligned} A_0^d &= f_A\left[v_L R_L^V + v_T R_T^V\right] \\ A_E^d &= f_A\left[v_L R_L^s + v_T R_T^{cs}\right] \\ A_M^d &= f_A v_T R_T^s \\ A_{A,T=1}^d &= f_A\left[(1-4\sin^2\theta_W)v_{T'}\left(\left(R_{LT}^A\right)^{10} + \left(R_{LT}^A\right)^{11}\right)\right] \\ A_{A,T=0}^d &= f_A\left[(1-4\sin^2\theta_W)v_{T'}\left(\left(R_{LT}^A\right)^{00} + \left(R_{LT}^A\right)^{01}\right)\right] \end{aligned} \quad (26)$$

and :

$$f_A = -\frac{G_F Q^2}{2\pi\sqrt{2}\alpha(v_L R_L^\gamma(\mathbf{q},\omega) + v_T R_T^\gamma(\mathbf{q},\omega))}$$

7 Electroweak radiative corrections

Precision on the violating asymmetry experiments is of the order of magnitude of higher order corrections, which have then to be taken into account. Besides the Born's approximation, several diagrams contribute up to a level of few % to the parity violating asymmetry. We divide these corrections in two kinds [7]. The fist one is related to the coupling between the exchanged boson and a single quark (other quarks being spectators). Diagrams of this

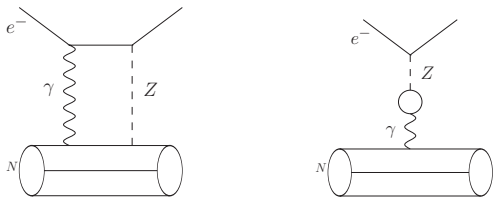

(a) γZ box. (b) γZ mixing.

Fig. 3. One quark electroweak corrections.

kind (see figure 3) lead to corrections to the asymmetry which can be calculated in the standard model. They are applied via the weak charge $Q_W = 1 - 4\sin^2\theta_W$ which becomes $Q_W = \rho'(1 - 4\kappa'\sin^2\theta_W)$ [21]. The effect on the asymmetry can be seen in the change the ξ parameters (see eq. 7 and 14) which are rewritten for the vector and axial part :

$$\begin{aligned} \xi_V^p &= \rho'_{eq}\left(1 + 4\hat{\kappa}'_{eq}\hat{s}_Z^2\right) - 2\left(2\lambda_{1u} + \lambda_{1d}\right) \\ \xi_V^n &= -\left[\rho'_{eq} + 2\left(\lambda_{1u} + 2\lambda_{1d}\right)\right] \\ \xi_V^{(0)} &= -\left[\rho'_{eq} + 2\left(\lambda_{1u} + \lambda_{1d} + \lambda_{1s}\right)\right] \end{aligned} \quad (27)$$

and :

$$\begin{aligned}\xi_A^{T=1} &= \frac{-2}{f_W}\left[\rho_{eq}\left(1-4\hat{\kappa}_{eq}\hat{s}_Z^2\right)-\left(\lambda_{2u}-\lambda_{2d}\right)\right]\\ \xi_A^{T=0} &= \frac{2\sqrt{3}}{f_W}\left(\lambda_{2u}+\lambda_{2d}\right)\\ \xi_A^{(0)} &= \frac{1}{f_W}\left[\rho_{eq}\left(1-4\hat{\kappa}_{eq}\hat{s}_Z^2\right)+2\left(\lambda_{2u}+\lambda_{2d}+\lambda_{2s}\right)\right]\end{aligned} \tag{28}$$

with the parameter values listed in table 2 [22] and where f_W defined in equation 20.

ρ'_{eq}	$\hat{\kappa}'_{eq}$	λ_{1u}	λ_{1d}	λ_{1s}	$\hat{s}_Z^2$
0.9875	1.0025	-1.810^{-5}	3.610^{-5}	3.610^{-5}	0.23119
ρ_{eq}	$\hat{\kappa}_{eq}$	λ_{2u}	λ_{2d}	λ_{2s}	
1.0004	1.0298	−0.0121	0.0026	0.0026	

Table 2. Standard model parameters for the neutral vector current in electron-hadron scattering.

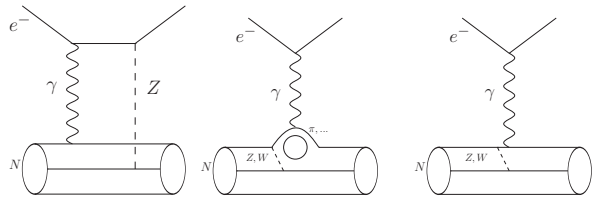

(a) Many quark radiative corrections (b) Anapole Moment

Fig. 4. Many quarks radiative corrections.

The second kind of radiative corrections involves several quarks. These corrections are calculated using models, as for the $N\pi$ fluctuation (fig. 4(a)) and have a large theoretical uncertainties. For the vector part, calculations show very small effect [7] which are not taken into account. For the axial part the dominating correction comes from the anapole moment (fig. 4(b)). Weak interaction among quarks in the nucleon can give axial-vector coupling between the virtual photon and the nucleon. Then a parity violating term arise in a purely electromagnetic process. The anapole moment has been evaluated in the $\overline{MS}$ scheme at $Q^2 = 0$ [23] :

$$\begin{aligned}R_A^{T=1} &= -0.0867 \pm 0.35\\ R_A^{T=0} &= 0.0144 \pm 0.2016\\ \xi_A^{T=1} &= -2\left(1+R_A^{T=1}\right) &&= -1.827 \pm 0.070\\ \xi_A^{T=0} &= R_A^{T=0} &&= 0.014 \pm 0.202\end{aligned} \tag{29}$$

These corrections have to be added to the one quark corrections.

The one quark corrections include vertex correction, correction to the propagator and correction on the γZ box diagrams at $Q^2 = 0$, but do not include two γ exchange, nor recent evolution on the γZ box diagrams. These last few years, numerous works on nucleon form factors have showed the importance of two γ exchange in elastic electron scattering for $Q^2 > 0.5\,(GeV/c)^2$, and recent studies [24,25] give the effect of 2 bosons exchange on the parity violating asymmetry (see fig.5). The correction is applied

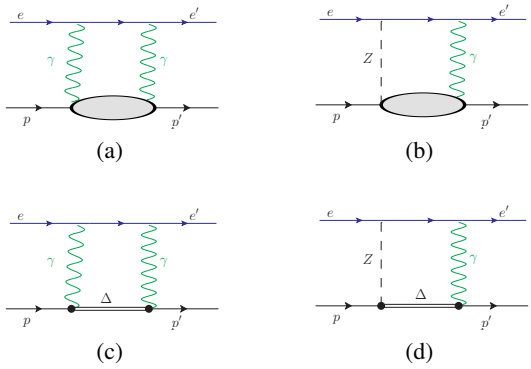

Fig. 5. Two bosons exchange (TBE) diagrams

.

as followed :

$$A_{Phys} = \frac{1}{1+\delta_{N+\Delta}} A_{Meas} \tag{30}$$

where $\delta_{N+\Delta}$ is the sum of δ_N for nucleon intermediate state (see fig. 5(a) and 5(b)) and δ_Δ for Δ intermediate state (see fig. 5(c) and 5(d)). The N and Δ contributions depend strongly on the kinematic (ϵ and Q^2). At small ϵ (large electron angle) the Δ contribution is very small, but dominate at forward angle. This leads to non trivial respective contribution, which needs to be correctly evaluated at the specific kinematics for each experiment.

This correction takes into account corrections already included in the one quark corrections. To avoid double counting, we have to used modified ρ' and κ' :

$$\begin{aligned}\rho'_{eq} &= \rho'^{PDG}_{eq}(1-\Delta\rho^{had}_{MS})\\ \kappa'_{eq} &= \kappa'^{PDG}_{eq}(1-\Delta\kappa^{had}_{MS})\end{aligned}$$

where ρ'^{PDG}_{eq} and κ'^{PDG}_{eq} are the standard model parameters [22], and $\Delta\rho^{had}_{MS} = 0.072\%$ and $\Delta\kappa^{had}_{MS} = 0.102\%$ are given in reference [24].

8 Experimental overview

Since fifteen years, several experiments have been dedicated to the study of the strange quark contribution in electromagnetic structure of the nucleon using parity violating asymmetry measurements in elastic eN and eD polarized

scattering. The experimental expression of the asymmetry can be written $A_{meas} = pA_{phys}$ where p is the polarization of the beam (between 0 and 1). The order of magnitude of A_{phys} is between $10^{-6} = 1ppm$ (ppm=parts per million=10^{-6}) and 60 ppm depending on the Q^2. To make asymmetry measurement at few percent statistic level, we need a large beam polarization, high luminosity and no intrinsic experimental asymmetry (no false asymmetry at the level of 0.1 ppm). One key element of such an experiment is the beam quality and polarization. Spin polarized electrons are produced by photoemission from various GaAs-based semiconductor photo-cathodes, using circularly polarized laser light [26,27]. Latest polarized electron source can provide up to 90% polarization. Beam polarization is usually measured after acceleration using a Møller polarimeter [28] each few days. To avoid any slow systematic drifts (like temperature sensitivity of the experimental setup, beam depolarization, etc...), helicity of the electron beam is reversed, at a frequency of few Hz using a randomly chosen pattern of helicity states. The electron beam current is changed by adjusting the laser power, typically ranging for parity violating experiment from 20 μA to 100 μA. The electron beam charge difference (as well as position differences) between helicity states are minimized using feedback on the laser beam (laser power for the charge and laser position on the photocathode for the beam position on target). We also measure beam angle difference at target in order to make corrections during the analysis. Order of magnitude of parameters differences is shown table 3 for G^0 backward angle.

Parameter	Jlab G0
A_Q	0.09 ± 0.08 ppm
Δx	−19 ± 3 nm
Δy	−17 ± 2 nm
$\Delta\theta_x$	−0.8 ± 0.2 nrad
$\Delta\theta_y$	0.0 ± 0.1 nrad
ΔE	2.5 ± 0.5 eV

Table 3. Parameters differences for G^0 backward experiment.

SAMPLE, HAPPEX and PVA4 have measured asymmetries on hydrogen and deuterium targets allowing the extraction of strange electric and magnetic contributions as well as axial form factor at $Q^2 = 0.1\,(GeV/c)^2$ (see figure 6). Recently new measurement from PVA4 on hydrogen allowed the strange vector contributions to be extract at $Q^2 = 0.22\,(GeV/c)^2$ (see figure 7).

SAMPLE experiment [29] took place at the MIT-Bates linear accelerator. It was using polarized electron beam of 40 μA at an energy of 125 and 200 MeV, with a maximum beam polarization of about 50%, on a 40 cm long hydrogen or deuterium target. Detector was a large air Čerenkov detector, and electrons scattered at 145° (backward angle) produced Čerenkov light measured by ten large diameter photomultipliers. The electric signal was integrated over the beam burst duration (25 μs). Measurement have been done at $Q^2 = 0.1\,(GeV/c)^2$ on both hydrogen and deuterium target in 1998-1999 [30,31,32,33]. In 2002, a new measurement has been done at $Q^2 = 0.04\,(GeV/c)^2$ on deuterium [34].

PVA4 experiment take place at MAMI with a 20 μA electron beam on 10 cm long hydrogen target. Beam energy was 570 MeV and 854 MeV and energy of scattered electrons were measured between 30° and 40° by lead fluoride (PbF_2) crystals. Once a crystal is fired, the signal is digitalized and a specific scaler corresponding to the integrated charge is incremented. Measurement of PV asymmetry has been done in 2000-2002 at $Q^2 = 0.23\,(GeV/c)^2$ [35], and in 2003 at $Q^2 = 0.108\,(GeV/c)^2$ [36]. In 2005, PVA4 collaboration was able to turn the detector in backward angle mode changing the target length to 23 cm to increase luminosity. A 315 MeV beam energy was used to measure the asymmetry on hydrogen at $Q^2 = 0.22\,(GeV/c)^2$ [37]. Beam polarizations of 70% and 80% were measured depending on the data setting. A new measurement on forward angle hydrogen is underway at $Q^2 = 0.62\,(GeV/c)^2$.

HAPPEX experiment runs in the Hall A of Jefferson Lab. It used 35 μA beam at about 3 GeV on hydrogen and helium target. Scattered electrons were detected in two high resolution spectrometers using a dedicated detection setup based on Čerenkov detection light emitted by the electrons. The light was collected by large diameter photomultipliers and integrated over 30 ms which was the duration of the helicity state. Hydrogen asymmetries have been measured at $Q^2 = 0.477\,(GeV/c)^2$ in 1998-1999 [38], and $Q^2 = 0.1\,(GeV/c)^2$ in 2005 [39]. A new measurement on hydrogen is underway at $Q^2 = 0.62\,(GeV/c)^2$. The original measurement of HAPPEX is the ^{4}He measurement. The elastic scattering on Helium (spin 0) is only sensitive to the electric form factor. A single elastic e-^{4}He asymmetry measurement provides directly the electric strange quark contribution :

$$A_{^4He} = \frac{G_F Q^2}{\sqrt{2}\pi\alpha}\left(\sin^2\theta_W + \frac{G_E^s}{2(G_E^{\gamma,p} + G_E^{\gamma,n})}\right) \qquad (31)$$

This equation is only valid at very low $Q^2 < 0.1\,(GeV/c)^2$. For higher momentum transfer, NN interactions are not negligible anymore and the asymmetry becomes sensitive to some $s\bar{s}$ pairs coming from NN interaction and not only from the nucleon itself. At $Q^2 \simeq 0.1\,(GeV/c)^2$ non nucleon $s\bar{s}$ pairs already contributes up to 15% [40]. Parity violating asymmetry on ^{4}He has been measured at $Q^2 = 0.077\,(GeV/c)^2$ in 2004-2005 [39].

Figures 6 and 7 show the results from these experiments at two Q^2 points. The strange quarks electric contribution is shown versus the strange quark magnetic contribution. One measurement give a linear combination of the two contributions (when using a calculation for the axial term) and is shown as a band using the experimental error. Forward angle on hydrogen, which is sensitive to both electric and magnetic strange contribution, corresponds to the diagonal band. The horizontal band on figure 6 is the helium HAPPEX experiment only sensitive to G_E^s and the almost vertical bands are backward angle hydrogen mainly sensitive to G_M^s. The whole data set at $Q^2 = 0.1$ has been

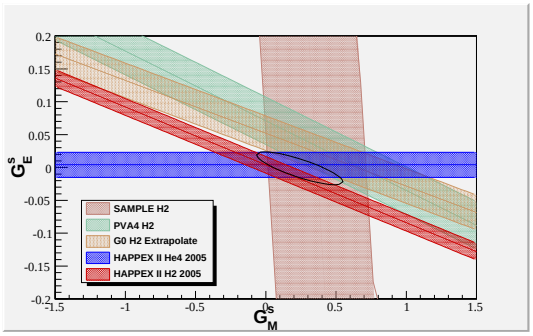

Fig. 6. Strange electric and magnetic contributions at $Q^2 = 0.1\,(GeV/c)^2$.

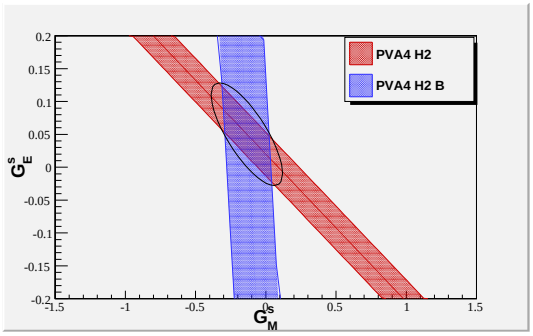

Fig. 7. Strange electric and magnetic contributions at $Q^2 = 0.22\,(GeV/c)^2$.

studied in [41] which provide world average values :

$$\begin{aligned} G_E^s(0.1) &= -0.006 \pm 0.016 \\ G_M^s(0.1) &= 0.33 \pm 0.21 \end{aligned} \tag{32}$$

which corresponds to 0.2% contribution of the proton electric form factor and to 3% contribution of the proton magnetic form factor. For $Q^2 = 0.22\,(GeV/c)^2$, only PVA4 provided data before G^0 , which leads to :

$$\begin{aligned} G_E^s(0.22) &= -0.050 \pm 0.038 \pm 0.019 \\ G_M^s(0.22) &= 0.14 \pm 0.11 \pm 0.11 \end{aligned} \tag{33}$$

given -3% contribution of the proton electric form factor and 2.9% contribution of the proton magnetic form factor. The G^0 experiment provides new measurements at $Q^2 = 0.22$ and $Q^2 = 0.63\,(GeV/c)^2$.

9 The G0 experiment

The G^0 experiment took place in the hall C of the Thomas Jefferson National Laboratory, located in Newport-News (Virginia, USA). It has a Continuous Beam Electron Facility (CEBAF) providing polarized electron beam up to 6 GeV (see fig. 8). Two linear accelerators, each with 160 supra-conducting cavities, can accelerate the electrons between 0.4 and 0.6 GeV, and recirculation arcs allow the electrons to make five passes. CEBAF is capable of simultaneous delivery of continuous beams to three end stations at a frequency of 499 MHz, each experimental hall having an electron burst every 2 ns. Each hall can choose his energy (varying the number of pass in the accelerator), his intensity (with a limit of 200 μA maximum total) and his helicity using control on the laser light of the polarized source. Since 2004, CEBAF is using a strained superlattice GaAs polarized source allowing more than 80% of beam polarization [26] which is measured before acceleration with a Mott polarimeter and at the hall C entrance using a møller polarimeter [28]. For G^0 experiment, helicity of the beam was changed at a frequency of 30 Hz (Macro Pulse MPS), and helicity pattern was randomly chosen from two sequences (quartet) of four MPS $(+--+)$ and $(-++-)$.

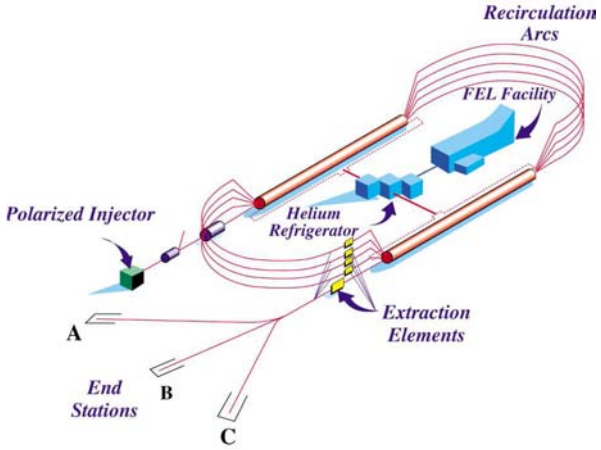

Fig. 8. CEBAF schematic.

The G^0 collaboration, which is about 70 physicists, built a dedicated full experimental setup to measure parity violating asymmetries at forward angle in a wide range of Q^2, and at backward angle on both hydrogen and deuterium targets for two different Q^2. A large toroidal supraconducting magnet has been built, covering the full angular acceptance around the beam axis to increase the statistics and remove possible azimuthal asymmetry (see figure 9). The target was 20 cm long and was filled either with liquid hydrogen, liquid deuterium or gazeous hydrogen for background measurement. The target's windows were contributing to the background and their thicknesses were minimized to reduce non elastic scattering in the detectors. The exit and entrance windows have the same shape to keep the target length constant when moving beam from the center. The high cryogenic power (450 W), allowed to run at high beam current (up to 60 μA).

9.1 The forward angle measurement

The scattered protons, in forward angle, was detected using scintillators array, located in the focal plane of the spectrometer in each of the 8 octants around the beam axis. Detector array were made of 16 plastic scintillators (16 FPDs for Focal plane Detectors) with different size in order to keep reasonable elastic proton rates (less than 1 MHz). The spectrometer was designed such that the magnetic field

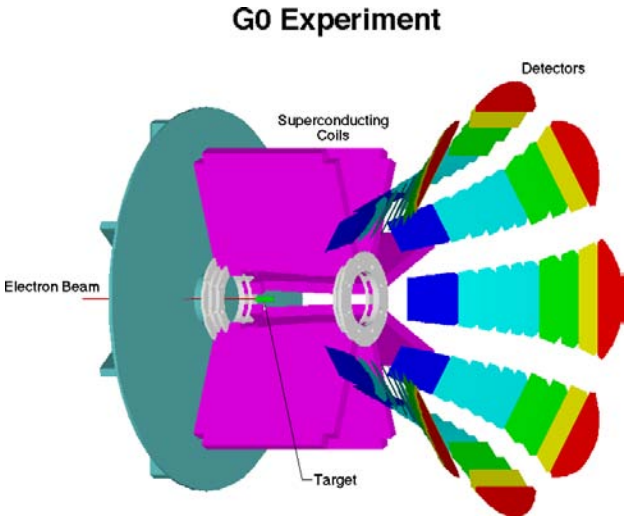

Fig. 9. Schematic view of G^0 .

was null on the beam axis, and focus a specific elastic proton kinematics to the same position on the focal plane, wherever the scattering take place along the target length (see fig. 10). The three sets of trajectories of figure 10 correspond to Q^2 from small (FPD 2) to large (FPD 15) detectors respectively for 0.128, 0.262 and 0.511 $(GeV/c)^2$. Neutral background coming from target were stopped using lead collimators and charged particles were selected using the FPDs. The wide G^0's acceptance at forward angle allowed us to measure elastic scattered protons for angles between 53° and 76° , corresponding to electron angles from 2° to 20° . All Q^2 from 0.12 to 1 $(GeV/c)^2$ were then measured separately, thanks to FPD's array, in one data taking.

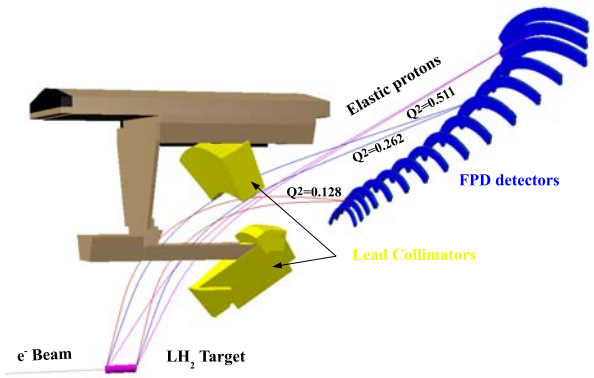

Fig. 10. Schematic view of G^0 at forward angle.

Each FPD was built with two layers of plastic scintillator, both of them seen by a 2 inches photomultiplier at both ends. The four signals were sent to constant fraction discriminators, and left and right signals were sent to a meantimer. A charged particle was selected using the coincidence of the front and back meantimers for which the time was measured relative to the beam burst. A specific scaler corresponding to this time of flight was then incremented. Half of the experiment got 24 scalers per FPD with a binning of 1 ns, the other half got 128 scalers with a binning of 0.25 ns. The typical time of flight spectra is shown fig. 11. To be able to do this time measurement, it was required a beam structure corresponding to one burst each 32 ns (instead of 2 ns as usual). Beam was then setup to 40 μA due to maximum instantaneous possible beam current in the accelerator. Time of flight spectra of all detectors were recorded for each helicity state at 30 Hz (for each MPS).

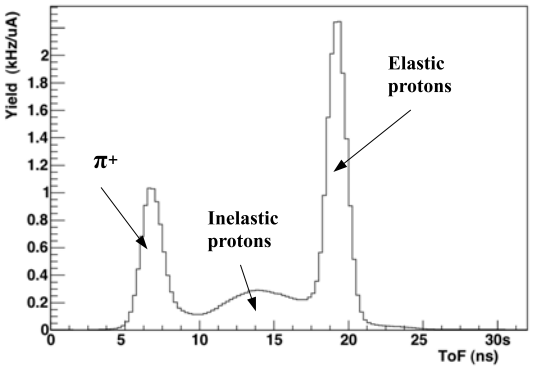

Fig. 11. Typical time of flight spectra for a FPD

The asymmetries were gotten using these time of flight spectra calculated within each quartet, selecting the elastic peak and subtracting inelastic background. The FPD 14 was splitted in two Q^2 points : 0.410 and 0.997 $(GeV/c)^2$. The FPD 15 has a wide elastic acceptance in Q^2 and was divided in three points : 0.511, 0.631 and 0.788 $(GeV/c)^2$. Results were published in 2005 [1]. Figure 12 shows the

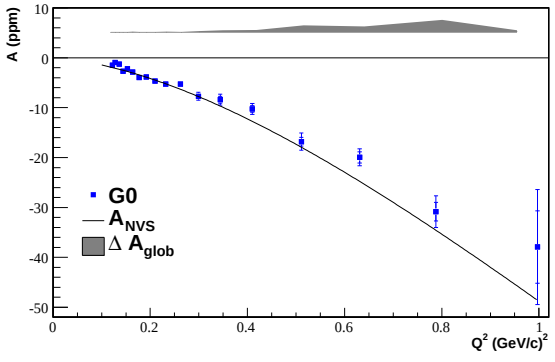

Fig. 12. Results of the forward angle experiment

physics asymmetries measured in forward angle mode. The inner error bars are statistical only, the outer ones are statistical plus systematic point to point. Global systematic errors are show in grey. The data points are compared with

the asymmetry from equation 21, calculated with no vector strange (NVS) contributions ($G_E^s = G_M^s = 0$), and with the axial form factor $G_A^{e,p}$ from equation 14 using theoretical radiative corrections (see section 7). To calculate A_{NVS} we choose the Kelly's parameterization of electromagnetic form factors (see section 4). The difference between the measurement and A_{NVS} is related to a linear combination of strange electric and magnetic contributions (using notation from eq.21) :

$$G_E^s + \eta G_M^s = \frac{A_{phy}^{exp} - A_{NVS}}{A_E^p} \text{ with } \eta = \frac{A_M^p}{A_E^p} \qquad (34)$$

These combinations versus Q^2 are showed figure 13 and present a non trivial electric and magnetic combination over the whole Q^2 range.

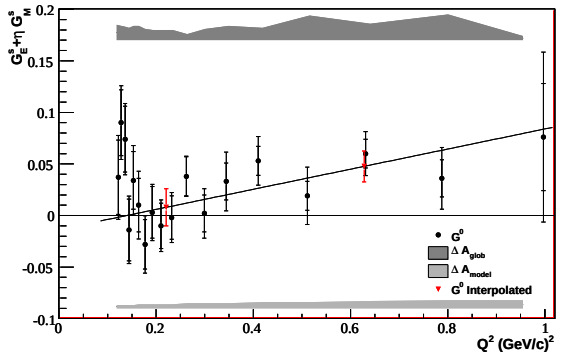

Fig. 13. Linear combination of strange electric and magnetic contributions from G^0 forward experiment [1].

9.2 Backward angle measurement

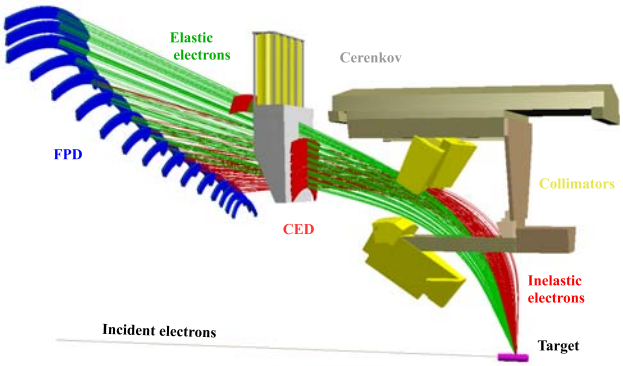

Fig. 14. Schematic view of G^0 at backward angle.

For the backward angle, the spectrometer and the FPDs were turn round. The elastic scattered electrons were detected at 110° . Because time of flight measurement did not help to discriminate elastic and inelastic electrons, we have added a new scintillators array at the exit of the cryostat (9 Cryostat Exit Detectors CED) to separate inelastic using trajectography. Elastic and inelastic electrons going through the same CED, fired a different FPD. Each CED was built with one layer of plastic scintillator seen at both ends by 2 inches photomultipliers. The photomultiplier's signals were discriminated using constant fraction discriminators and sent to a meantimer to make the left-right coincidence. A specific electronics was built to provide the coincidence of the 14 FPDs (the first 2 FPDs were unused) and 9 CEDs and record the counting using high speed scalers (one for each FPD/CED cell). Quasi-elastic scattering on deuterium target was also performed. To reject the π^- background coming from inelastic scattering on neutron, we built an aerogel Čerenkov, covering the same acceptance than the CEDs, for which the pion threshold (570 MeV) was above pion momentum in G^0 backward measurement. Electrons passing through 5.2 cm thick silica aerogel (refraction index of 1.03) create Čerenkov light which was detected by four large diameter (5 inches) photomultipliers. The CED-FPD coincidence electronics was duplicated to measure scattered electrons in coincidence with the Čerenkov : the electron matrix (see fig. 15), and inelastic scattered pions when Čerenkov was missing : the pion matrix. We measure the parity violating asymmetries

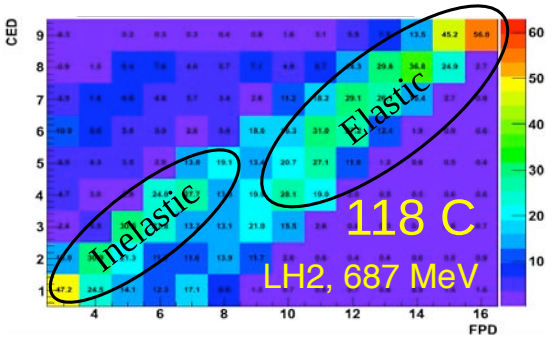

Fig. 15. Electron CED/FPD matrix showing elastic on the right and inelastic on the bottom left.

on both hydrogen and deuterium targets at two Q^2 : 0.22 and 0.63 $(GeV/c)^2$. At backward angle, the spectrometer's acceptance in Q^2 is very small, and since the scattered angle is fixed by the experimental setup, we needed to change the beam energy in order to change the Q^2. Data was taken between March 2006 and April 2007 using an energy of 362 Mev for the lower Q^2, and 687 MeV for the upper one. We used a beam current of 60 μA for the hydrogen data at low and high energy, whereas beam current has been lowered respectively to 35 and 20 μA for deuterium target, to keep reasonable rates in the individual detectors. Since no time of flight information were required for background discrimination, we use the standard 2 ns beam structure of CEBAF, excepted for some dedicated background study

data taking. The summary of data taking is listed in table 4.

	Charge (C)	I (μA)	A_{meas} (ppm)	$\delta A/A$
LH_2 362 MeV	90	60	-9.72 ± 0.87	9%
LD_2 362 MeV	70	35	-13.50 ± 0.81	6%
LH_2 687 MeV	120	60	-36.9 ± 2.43	6.7%
LD_2 687 MeV	45	20	-37.4 ± 3.34	8.9%

Table 4. Accumulated statictics for G^0 backward for all target/energy.

Asymmetries, within quartet helicity structure, were calculated for each cell of the matrices, from the coincidence rates recorded MPS by MPS and normalized to the beam current. The asymmetries for each matrix cells were then averaged over the run duration. The final asymmetry was evaluated by the weighted average over the whole data taking and all CED-FPD cells where elastic scattering dominate (the elastic locus).

The analysis is divided into three steps. In the first step, corrections were applied to the yield MPS by MPS, for electronics effects, such as deadtime, random coincidences and pion contamination. An error on this correction has been calculated and is applied on the final asymmetry. While most of the corrections were done MPS by MPS, a residual asymmetry, from such effect not corrected on the yield, exists and was also corrected on the final asymmetry. The remaining residual asymmetry and the error associated to the MPS by MPS corrections are :

$$\begin{aligned} &\text{H 362 MeV}: \quad A_{rates} = -0.31 \pm 0.08 \pm 0 \text{ ppm} \\ &\text{D 362 MeV}: \quad A_{rates} = -0.58 \pm 0.21 \pm 0 \text{ ppm} \\ &\text{H 687 MeV}: \quad A_{rates} = -1.28 \pm 0.18 \pm 0 \text{ ppm} \\ &\text{D 687 MeV}: \quad A_{rates} = -7.0 \pm 1.8 \pm 0 \text{ ppm} \end{aligned} \tag{35}$$

where the uncertainties are point to point and global systematic.

In the second step, the background in the elastic locus, which is about 10% to 15% for all targets and energies (see table 5), is subtracted. The dominant contribution comes from quasi elastic scattering on the aluminum windows of the target. The yield of this background has been

Target / Q^2	f_{al} %	f_{π^-} %	f_{other} %	f_{total} %
H / 0.221	12.9 ± 6.4	0 ± 0.1	0.3 ± 0.3	13.2 ± 6.4
D / 0.221	9.9 ± 5.0	0 ± 0.2	0.5 ± 0.5	10.4 ± 5.0
H / 0.628	11.0 ± 5.5	0 ± 0.1	2.3 ± 2.3	13.3 ± 6.0
D / 0.628	6.1 ± 3.1	4 ± 1.5	2.9 ± 2.9	13 ± 4.5

Table 5. Background fraction. From left to right, contributions come from : Aluminum of target windows (al), misidentified π^- and sum of π^0 and inelastic electrons (other).

determined using empty target data, and the asymmetry is reasonably assumed to be the same than the deuteron one (in the static approximation). To take nuclear effects into account we add a 5% error on this asymmetry. Remaining backgrounds are π^- contamination, π^0 decay and inelastic electrons. Rates of misidentified π^- fraction were determined using time of flight measurement and pulse shape analysis of Čerenkov photomultiplier during diagnostic measurements. Their asymmetry was measured using the pion matrix. The electron inelastic rates were determined using comparison between data taken in a wide range of magnetic field settings and the simulation, leading to a very small contribution (<0.1%) for which 100% error has been taken. Their asymmetry was measured using the electron's matrix within the inelastic locus (see figure 15, to be published). At least, π^0 rates were small, error of 100% has been taken for them, and their asymmetry were measured in the upper left side of the electron's matrix. Finally background asymmetry correction and associated errors are :

$$\begin{aligned} &\text{H 362 MeV}: \quad A_{bckg} = +0.5 \pm 0.11 \pm 0.40 \text{ ppm} \\ &\text{D 362 MeV}: \quad A_{bckg} = -0.07 \pm 0.02 \pm 0.08 \text{ ppm} \\ &\text{H 687 MeV}: \quad A_{bckg} = -0.1 \pm 0.61 \pm 0.86 \text{ ppm} \\ &\text{D 687 MeV}: \quad A_{bckg} = -2. \pm 0.48 \pm 0.23 \text{ ppm} \end{aligned} \tag{36}$$

Two other corrections have to be applied to the asymmetries. The first one is the external and internal radiative corrections [42] which were calculated using the simulation of the complete G^0 setup, using GEANT3 package, and have been applied on the experimental asymmetries comparing simulation with and without radiative corrections. The last correction is the two bosons exchange correction [24] (see eq. 30), for which the specific correction for G0 are:

MeV	radiative corrections	$\delta_{N+\Delta}$ (%)
H 362 MeV:	$1.037 \pm 0.002 \pm 0$	1.46 ± 0.2
D 362 MeV:	$1.032 \pm 0.002 \pm 0$	0.5 ± 0.2
H 687 MeV:	$1.037 \pm 0.002 \pm 0$	0.68 ± 0.2
D 687 MeV:	$1.034 \pm 0.002 \pm 0$	1.19 ± 0.2

(37)

The beam polarization has been measured weekly using a Møller polarimeter at high energy and a Mott polarimeter for low energy. At the end, a unique polarization value, averaged over the entire experiment, was used. A additional systematic error has been added for the low energy, because the Møller polarimeter was not useable :

$$\begin{aligned} &\text{362 MeV}: \quad P_e = 85.8 \pm 2.1 \pm 1.4\% \\ &\text{687 MeV}: \quad P_e = 85.8 \pm 1.4 \pm 1.4\% \\ &A_{phys} = \frac{1}{P_e} A_{meas} \end{aligned} \tag{38}$$

The Q^2 for each data set has been calculated using a simulation of the complete G^0 setup (see table 6), and includes errors on detector position, beam energy and magnetic field of G^0, leading to about 0.5% uncertainty. The beam energy was measured for each settings and typical uncertainties of about 0.14% was reached.

From the measured asymmetries listed in table 4, applying additive corrections from equation 35 and equation

36, and multiplicative ones from equation 38 and equation 37, we got the final physics parity violating asymmetries as shown in table 6 [43].

Target	E_{beam} GeV	Q^2 GeV^2	A_{phys} ppm
H	0.359	0.2217	$-11.25 \pm 0.86 \pm 0.27 \pm 0.43$
D	0.360	0.2193	$-16.93 \pm 0.81 \pm 0.41 \pm 0.21$
H	0.682	0.6264	$-45.9 \pm 2.4 \pm 0.80 \pm 1.$
D	0.686	0.6294	$-55.5 \pm 3.3 \pm 2. \pm 0.7$

Table 6. Final physics asymmetries for G^0 backward angle experiment. The uncertainties are statistical, point to point systematic and global systematic.

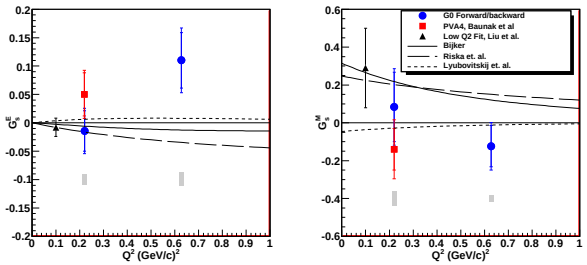

Fig. 17. Electric and magnetic strange contributions to nucleon's form factors, compared to a small set of models (see text).

10 Strange quark contributions

Using the physics asymmetries measured in forward and backward angle, we can determine the strange quarks contribution to the nucleon form factors as well as the isovector axial form factor in electron scattering. Common Q^2 were defined by averaging the Q^2 from hydrogen and deuteron backward angle measurements : $Q^2 = 0.221$ and $Q^2 = 0.628\,(GeV/c)^2$. The forward angle results were then interpolated to these Q^2, using the linear combination $G_E^s + \eta G_M^s$ defined in equation 34. The results of this interpolation is shown Figure 13 with the diamond points which are the forward angle interpolated at backward Q^2 values. Associated errors have been taken to 70% of the nearest point. Kelly's form factor parameterization has been used to extract strange quark contribution to be consistent with the deuteron model. For the proton form factors, uncertainty of 1% has been taken for the magnetic, and uncertainties of 0.5% and 1% have been taken for the electric one depending on Q^2 (respectively 0.22 and 0.63 (GeV/c)^2). For the neutron form factors, 2% has been taken for the magnetic and respectively 5.7% and 7.3% for the electric one.

The two vector form factors G_E^s, G_M^s are shown in figure 16, with our new G^0 results (circle points) which includes statistic (inner) plus systematic (outer) errors. Global systematic errors are shown with the grey square. Also shown is the last PVA4 point (square) [37] and a global fit of all the low Q^2 asymmetries [41] (triangle). While strange quark can contribute to intrinsic nucleon's magnetic moment μ_N, given a non zero value of G_M^s at $Q^2 = 0$, the strange electric contribution G_E^s vanish at $Q^2 = 0$ since there is no intrinsic strangeness in the nucleon.

On this figure, three different approaches based on Lattice QCD calculations are shown. The error band limited by the dashed dotted line [44], shows very small electric and magnetic contribution compatible with zero for all Q^2. The second model [45], with the error band represented by the solid line, predicts positive non zero values for the electric strange quark contribution and positive but compatible with zero for the magnetic one. The last lattice model, corresponding to the open triangles [46,47,48], shows only one Q^2 calculation for the electric term which is compatible with zero, and two Q^2 calculations for the magnetic

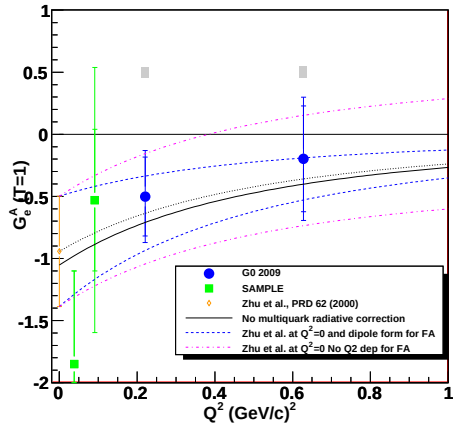

Fig. 18. Axial form factors as seen in electron elastic scattering.

one given small non zero value but with an opposite sign compared to the solid line one. For G_E^s, while the experimental average value at $Q^2 = 0.1$ is small, form factors extracted from PVA4 [37] and G^0 , at $Q^2 = 0.22$ and $Q^2 = 0.63\,(GeV/c)^2$, seems to indicate a positive electric strange quark contribution up to 0.6 $(GeV/c)^2$, in agreement with the model from Lewis [45]. For G_M^s, our data which are compatible with zero at both Q^2 while the average value at $Q^2 = 0.1$ are in favor of a large positive G_M^s at $Q^2 = 0$, suggests a magnetic contribution decreasing relatively quickly to zero above 0.1 $(GeV/c)^2$.

Figure 17 shows the same data with three other models. The dot line is based on the perturbative chiral quark model at one loop [49] and predicts a positive G_E^s but too small at high Q^2 compared to our data, and a negative G_M^s at $Q^2 = 0$ contrary to what suggest the low $Q^2 = 0.1$ global fit. The long dashed line [50] is based on a simple quark model and predicts opposite sign compared to G^0 data at high Q^2. The sign and the size of G_M^s agree with the data at low Q^2 but does not vanish quickly enough as suggested by our data. The last model [51], represented by the solid line, is based on a Vector Dominance Model, consisting in three quark intrinsic structure, surrounded by a meson cloud and has pretty much the same behavior than the previous simple quark model.

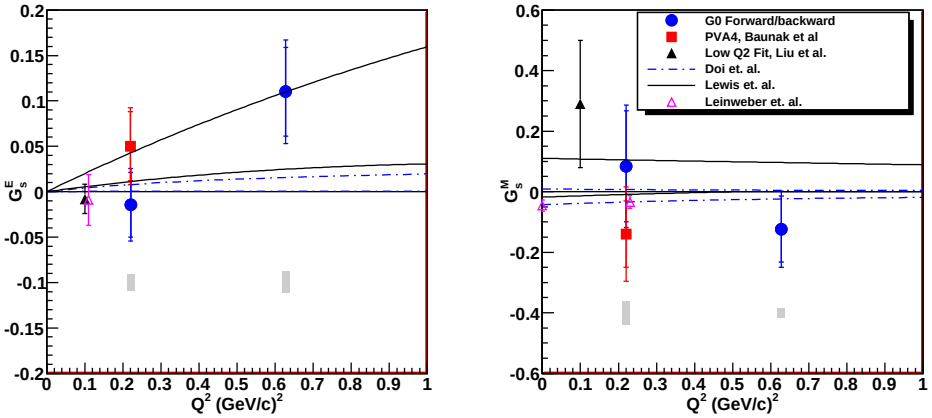

Fig. 16. Electric and magnetic strange contributions to nucleon's form factors, compared to a small set of lattice calculations.

Figure 18 shows our results on the isovector axial form factor as seen in elastic electron scattering. It differs from the isovector axial form factor using neutrino scattering by precise one-quark radiative corrections and mostly unknown multi-quarks corrections (see eq. 14 and section 7). Our data (filled circles) along with the previous SAMPLE results [32,34] (squares) are compared to the axial isovector form factor including only the one-quark radiative corrections (solid line) and including both one-quark and multi-quark corrections (dot line). The open diamond is the full calculation [23], existing only for $Q^2 = 0$ and including theoretical errors on multi-quark corrections (see eq. 29). Since we have no theoretical indication about the Q^2 dependance of the multi-quark radiative corrections, different assumption have been made. The inner dashed lines shows a standard dipole dependance (using axial mass M_A from neutrino scattering) associated to the error at $Q^2 = 0$. The dot-dashed lines shows the error band if we assume that these corrections have no Q^2 dependance. This is the first experimental measurement of the Q^2 dependance of the isovector axial form factor in electron scattering. While the precision of the data prevent us to draw any quantitative conclusion, the measurement agrees with the calculated radiative corrections.

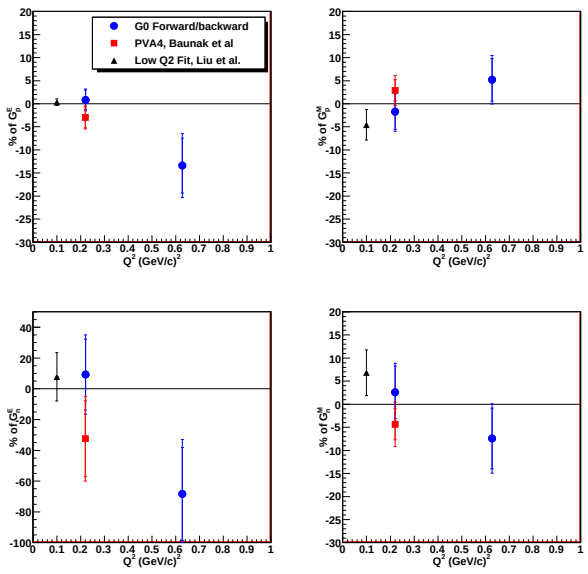

Fig. 19. Electric (left) and magnetic (right) contribution of the strange quarks to the electromagnetic form factors of the proton (above) and neutron (below) in percent

Finally figure 19 show the contributions of the strange quarks to the electric and magnetic form factors of the proton and neutron. The net contribution of the strange quark, which is $-\frac{1}{3}G^s_{E,M}$ (see eq. 5), is shown figure 19 where both the electric (left) and magnetic (right) contributions are expressed in percent. The two upper graph shows contribution to the proton, the two lower ones to the neutron. This shows a large contribution on the electric term for high Q^2 with about 15% contribution to the proton and 70% contribution to the neutron, but with large errors. New measurements at $Q^2 = 0.6\,(GeV/c)^2$ from HAPPEX and PVA4 at forward angle will possibly decrease the error bar in a near future.

11 conclusion

The G^0 experiment has measured parity violating asymmetries in elastic and quasi-elastic scattering on proton and deuteron. In addition of the measurements done in forward angle configuration, new measurements at backward electron angle on both hydrogen and deuterium target are presented. This allows the direct determination of the strange quark contributions to the vector electromagnetic form factors and the axial form factor as measured in electrons scattering at two Q^2 : 0.22 and 0.63 $(GeV/c)^2$. Experimental setup is presented and the results are compared to previous experiments and a small set of recent theoretical predictions. The results agree with calculations for the axial part and show a possible non negligible contribution of the

strange quarks to the electric nucleon's form factor for the high Q^2. On the other hand strange quark magnetic contribution is compatible with zero at both momentum transfers. New measurements will be done at 0.63 $(GeV/c)^2$ by HAPPEX and PVA4 experiments , which should better constraint the strange quark's contribution.

References

1. D.S. Armstrong et al. (G0), Phys. Rev. Lett. **95**, 092001 (2005)
2. D. Drechsel, Brazilian Journal of Physics **24**(2), 590 (1994)
3. G.A. Miller, Phys. Rev. C **57**(3), 1492 (1998)
4. J. Arrington, W. Melnitchouk, J.A. Tjon, Physical Review C (Nuclear Physics) **76**(3), 035205 (11) (2007)
5. S. Galster et al., Nucl. Phys. **B32**, 221 (1971)
6. J.J. Kelly, Phys. Rev. **C70**, 068202 (2004)
7. M.J. Musolf, T.W. Donnelly, J. Dubach, S.J. Pollock, S. Kowalski, E.J. Beise, Physics Reports **239**(1-2), 1 (1994), ISSN 0370-1573
8. E. Leader, A.V. Sidorov, D.B. Stamenov, Phys. Rev. **D67**, 074017 (2003)
9. A. Bodek, S. Avvakumov, R. Bradford, H.S. Budd, Eur. Phys. J. **C53**, 349 (2008)
10. D.B. Day et al., Phys. Rev. Lett. **59**, 427 (1987)
11. D.B. Day, J.S. McCarthy, T.W. Donnelly, I. Sick, Ann. Rev. Nucl. Part. Sci. **40**, 357 (1990)
12. J. Arrington et al., Phys. Rev. Lett. **82**, 2056 (1999)
13. L. Diaconescu, R. Schiavilla, U. van Kolck, Phys. Rev. C **63**(4), 044007 (2001)
14. R. Schiavilla, J. Carlson, M.W. Paris, Phys. Rev. **C67**, 032501 (2003)
15. R. Schiavilla, J. Carlson, M.W. Paris, Phys. Rev. **C70**, 044007 (2004)
16. R.B. Wiringa, V.G.J. Stoks, R. Schiavilla, Phys. Rev. **C51**, 38 (1995)
17. B. Desplanques, J.F. Donoghue, B.R. Holstein, Annals of Physics **124**(2), 449 (1980), ISSN 0003-4916
18. A. De Pace, EDS.S.BOFFI ET AL p. 166 (1996)
19. M.B. Barbaro, A.D. Pace, T.W. Donnelly, A. Molinari, Nuclear Physics A **598**(4), 503 (1996), ISSN 0375-9474
20. A. Meucci, C. Giusti, F.D. Pacati, Nuclear Physics A **756**(3-4), 359 (2005), ISSN 0375-9474
21. W.J. Marciano, A. Sirlin, Phys. Rev. D **29**, 75 (1984)
22. C. Amsler et al. (Particle Data Group), Phys. Lett. **B667**, 1 (2008)
23. S.L. Zhu, S.J. Puglia, B.R. Holstein, M.J. Ramsey-Musolf, Phys. Rev. **D62**, 033008 (2000)
24. J.A. Tjon, P.G. Blunden, W. Melnitchouk, Physical Review C (Nuclear Physics) **79**(5), 055201 (12) (2009)
25. K. Nagata, H.Q. Zhou, C.W. Kao, S.N. Yang, Physical Review C (Nuclear Physics) **79**(6), 062501 (5) (2009)
26. C.K. Sinclair, P.A. Adderley, B.M. Dunham, J.C. Hansknecht, P. Hartmann, M. Poelker, J.S. Price, P.M. Rutt, W.J. Schneider, M. Steigerwald, Phys. Rev. ST Accel. Beams **10**(2), 023501 (2007)
27. J. Hansknecht, M. Poelker, Phys. Rev. ST Accel. Beams **9**(6), 063501 (2006)
28. J.M. Grames, C.K. Sinclair, J. Mitchell, E. Chudakov, H. Fenker, A. Freyberger, D.W. Higinbotham, M. Poelker, M. Steigerwald, M. Tiefenback et al., Phys. Rev. ST Accel. Beams **7**(4), 042802 (2004)
29. E.J. Beise, M.L. Pitt, D.T. Spayde, Prog. Part. Nucl. Phys. **54**, 289 (2005)
30. D.T. Spayde et al. (SAMPLE), Phys. Rev. Lett. **84**, 1106 (2000)
31. R. Hasty et al. (SAMPLE), Science **290**, 2117 (2000)
32. D.T. Spayde (SAMPLE), Eur. Phys. J. **A24S2**, 51 (2005)
33. D.T. Spayde et al. (SAMPLE), Phys. Lett. **B583**, 79 (2004)
34. T.M. Ito et al. (SAMPLE), Phys. Rev. Lett. **92**, 102003 (2004)
35. F.E. Maas et al. (A4), Phys. Rev. Lett. **93**, 022002 (2004)
36. F.E. Maas et al., Phys. Rev. Lett. **94**, 152001 (2005)
37. S. Baunack et al., Phys. Rev. Lett. **102**, 151803 (2009)
38. K.A. Aniol et al. (HAPPEX), Phys. Rev. **C69**, 065501 (2004)
39. A. Acha et al. (HAPPEX), Phys. Rev. Lett. **98**, 032301 (2007)
40. M.J. Musolf, R. Schiavilla, T.W. Donnelly, Phys. Rev. C **50**(4), 2173 (1994)
41. J. Liu, R.D. McKeown, M.J. Ramsey-Musolf, Physical Review C (Nuclear Physics) **76**(2), 025202 (8) (2007)
42. Y.S. Tsai, slac-pub-0848 (1971), lectures given at 'Nato Advanced Inst. on Electron Scattering and Nuclear Structure, Cagliari, Italy, 1970
43. D. Androić et al., to be published (2009)
44. T. Doi, M. Deka, S.J. Dong, T. Draper, K.F. Liu, D. Mankame, N. Mathur, T.S. χQCD Collaboration (χQCD Collaboration), Physical Review D (Particles and Fields) **80**(9), 094503 (6) (2009)
45. R. Lewis, W. Wilcox, R.M. Woloshyn, Phys. Rev. D **67**(1), 013003 (2003)
46. D.B. Leinweber, S. Boinepalli, I.C. Cloet, A.W. Thomas, A.G. Williams, R.D. Young, J.M. Zanotti, J.B. Zhang, Phys. Rev. Lett. **94**(21), 212001 (2005)
47. D.B. Leinweber, S. Boinepalli, A.W. Thomas, P. Wang, A.G. Williams, R.D. Young, J.M. Zanotti, J.B. Zhang, Physical Review Letters **97**(2), 022001 (4) (2006)
48. P. Wang, D.B. Leinweber, A.W. Thomas, R.D. Young, Physical Review C (Nuclear Physics) **79**(6), 065202 (7) (2009)
49. V.E. Lyubovitskij, P. Wang, T. Gutsche, A. Faessler, Phys. Rev. **C66**, 055204 (2002)
50. D.O. Riska, B.S. Zou, Phys. Lett. **B636**, 265 (2006)
51. R. Bijker, Eur. Phys. J. **A32**, 403 (2007)